The Central Mongolia Seismic Experiment: Multiple Applications of Temporary Broadband Seismic Arrays

by Anne Meltzer, Joshua C. Stachnik, Demberel Sodnomsambuu, Ulziibat Munkhuu, Baasanbat Tsagaan, Mungunsuren Dashdondog, and Raymond Russo

ABSTRACT

As part of multidisciplinary research on intracontinental deformation and surface uplift, we deployed a temporary broadband seismic array in central Mongolia covering an ~900 × 600 km area extending from Lake Khövsgöl in the north to the Altai Mountains in the south. A total of 112 broadband stations were deployed as three separate subarrays in two separate mobilizations. Each subarray recorded local, regional, and teleseismic earthquakes for a 21-month period. Although the primary purpose of the array is to characterize the lithosphere and sublithospheric mantle, the array recorded a number of events of potential interest to the broader geoscience community including the Chelyabinsk meteor explosion, North Korean nuclear tests, the deep M_w 8.3 Sea of Okhotsk earthquake, and large megathrust events offshore Chile and in Nepal. The array includes the first dense deployment of seismometers across the Hangay dome, a region previously believed to be relatively aseismic serving as a rigid block focusing strain to the west and south along the Mongolian and Gobi-Altai. Initial results from local earthquakes recorded by the array suggest that the Hangay is deforming rather than behaving as a rigid block and that the earthquake potential of faults within the Hangay should be incorporated in hazard analysis for Mongolia.

Supplemental Content: Table of station location, sensor type, data range and recovery, sensor orientation, data quality, and site characteristics, and figures showing subarrays and station names of the central Mongolia seismic experiment plotted on Google Earth, and a plot of sensor orientation and histogram of uncertainty.

INTRODUCTION

Mongolia sits deep in the Asian continental interior between the Siberian craton to the north, the diffuse northern edge of deformation associated with the India–Asia collision to the south, and far-field subduction of the Pacific plate to the east (Fig. 1). Central and western Mongolia constitute a significant portion of the greater Mongolian plateau, an ~2.6 million km^2 area of central Asia with an average elevation of ~1500 m. High-elevation low-relief surfaces are common on continents but are not predicted by plate tectonics. The origin and persistence of continental plateaus through time provides insight into the evolution of continents and interactions between mantle dynamics and surface processes. These large-scale topographic features impact the geologic record, climate, and biogeography. The high topography of the Mongolian plateau has been attributed to far-field effects of India–Asia convergence, Pacific plate subduction, mantle plume activity, convective mantle flow, and magmatic underplating (Molnar and Tapponnier, 1975; Windley and Allen, 1993; Cunningham, 2001; Petit *et al.*, 2002, 2008; Yanovskaya and Kozhevnikov, 2003; Bayasgalan *et al.*, 2005; Zorin *et al.*, 2006). Within central Mongolia, the broad domal Hangay upland (~200, 000 km^2) is embedded in the greater Mongolian plateau. Elevations within the Hangay average 2500 m, approximately 1000 m above the regional trend. Locally, the highest peak Otgontenger reaches just over 4000 m. The drainage divide in the Hangay separates rivers flowing north to the Arctic Ocean from those flowing into internally drained basins to the west and south.

A kinematic transition between predominantly compressional deformation to the south and extension adjacent to the Siberian craton takes place in Mongolia. In western Mongolia, northward-directed shortening related to the India–Asia collision decreases from south to north from ~10 mm/yr south of the Altai, to ~4 mm/year in the Altai, and to 0 on the Siberian craton (Calais *et al.*, 2003). Central and eastern Mongolia moves eastward at ~4mm/yr (Calais *et al.*, 2003). Major strike-slip faults within Mongolia accommodate the transition from shortening to extension and give rise to the Mongolian

doi: 10.1785/0220180360

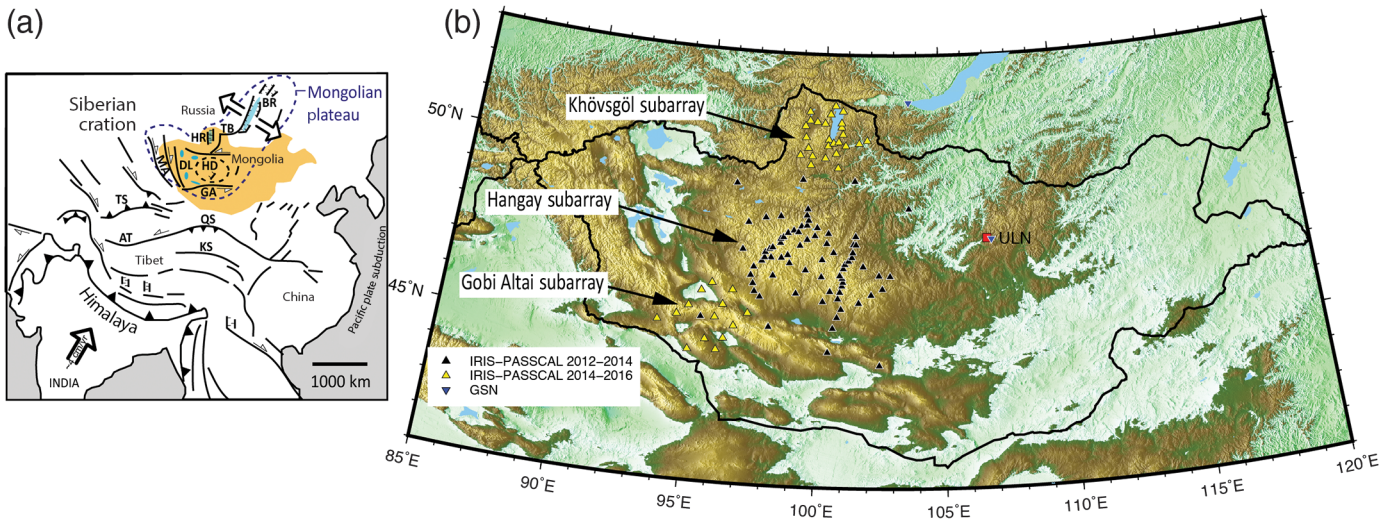

▲ **Figure 1.** (a) Tectonic setting of Mongolia. AT, Altyn Tagh; BR, Baikal rift; DL, Mongolian depression of lakes; GA, Gobi-Altai; HD, Hangay dome; HR, Khövsgöl rift; KS, Kunlun Shan; MA, Mongolian Altai; QS, Qilian Shan; TB, Tunka basin; TS, Tien Shan. (b) Station locations central Mongolia seismic experiment, subarrays, and Global Seismic Network station ULN. More detailed station location maps including station names are included in Ⓔ Figure S1 (available in the supplemental content to this article). The color version of this figure is available only in the electronic edition.

and Gobi-Altai ranges. The Bulnay and Gobi-Altai fault systems have sustained some of the largest recorded intracontinental earthquakes, four events **M** ≥ 8.0 within a 53 yr period in the early-to-mid-1900s (Tapponnier and Molnar, 1979; Khil'ko *et al.*, 1985; Baljinnyam *et al.*, 1993; Schlupp and Cisternas, 2007). Extension is accommodated by the Baikal, Tunka, Khövsgöl, Darkhad, and Busiingol rifts that wrap around the southern and eastern margin of the Siberian craton (Fig. 1).

Mongolia has a complex geologic history. The crust is composed of Archean to early Proterozoic crystalline rocks modified by Paleozoic accretionary events associated with formation of the central Asian orogenic belt, a protracted and significant period of continental growth involving the opening and closing of ocean basins in the Neoproterozoic and early Phanerozoic (1000–250 Ma; Şengör *et al.*, 1993; Badarch *et al.*, 2002; Jahn, 2004; Windley *et al.*, 2007; Wilhem *et al.*, 2012). The accreted terranes of Mongolia sit between the Siberian craton to the north and the Tarim and North China cratons to the south. Younger Cenozoic deformation and basalt volcanism continues today. The elevated low-relief landscape hosts a 30 Ma record of intermittent basalt magmatism sourced from the sublithospheric mantle (Barry *et al.*, 2003; Yarmolyuk *et al.*, 2008; Hunt *et al.*, 2012; Ancuta *et al.*, 2014; Carlson and Ionov, 2014; Ancuta *et al.*, 2018). A number of these basalts contain mantle and lower crustal xenoliths (Stosch *et al.*, 1995; Ionov, 2007; Carlson and Ionov, 2014).

As part of a larger multidisciplinary project investigating the origin of high topography in continental interiors, we deployed temporary broadband seismic stations from 2012 to 2016 to determine the structure and composition of the lithosphere and sublithospheric mantle beneath the region. The deployment is a collaborative effort between Lehigh University, the University of Florida, and the Institute of Astronomy and Geophysics, Mongolian Academy of Sciences. The central Mongolia seismic experiment consists of 112 broadband seismic stations in two separate deployments covering an ~900 × 600 km region in central Mongolia (Fig. 1). Although the primary purpose of the seismic experiment is to look at crustal and upper-mantle structure, the data recorded by the array are applicable to a number of studies. Local and regional earthquakes recorded by the array can be used to improve seismic hazard assessment in Mongolia. Data recorded by the array fill a significant gap in existing regional velocity and attenuation tomographic models for central and eastern Asia and can be used to improve geodynamic models and nuclear monitoring capabilities in this part of the world. Central Mongolia is antipodal to South America providing a window into deep Earth structure (Rial and Cormier, 1980; Butler *et al.*, 1986; Poupinet *et al.*, 1993; Butler and Tsuboi, 2010; Retailleau *et al.*, 2014). Data recorded by the array have the potential to contribute to studies of surface and atmospheric processes. A number of the stations are located along rivers in the Hangay and Altai ranges and can be used to study fluvial processes and erosion (Burtin *et al.*, 2008; Hsu *et al.*, 2011; Schmandt *et al.*, 2013; Roth *et al.*, 2014). Central Mongolia is a major site of cyclogenesis in the lee of the Sayan, Hangay, and Altai ranges linked to loess deposition in China and midwinter storms in the North Pacific (Chung *et al.*, 1976; Adachi and Kimura, 2007; Roe, 2009; Penny *et al.*, 2010; Caves *et al.*, 2015). Within the time period of the two deployments that make up the central Mongolia seismic experiment, we recorded a number of significant events: the Chelyabinsk meteor explosion in 2013, nuclear

tests by North Korea in 2013 and 2016, the deep 2013 M_w 8.3 Sea of Okhotsk earthquake and aftershock sequence, megathrust ruptures of the Chilean subduction zone in the 2014 Iquique M_w 8.2 and 2015 Illapel M_w 8.3 earthquakes, and the 2015 M_w 7.8 Gorkha earthquake in Nepal.

In this article, we give a complete description of the central Mongolia seismic experiment, provide an overview of the data acquired, data quality, and noise characteristics, review events of interest recorded by the array, and present preliminary results of local seismicity in the Hangay.

INSTRUMENT DEPLOYMENT

A total of 112 broadband seismic stations were deployed in central Mongolia, extending from the Lake Khövsgöl region near the Mongolia–Russia border, through the Hangay dome region, and into the Gobi-Altai region near the Mongolia–China border (Fig. 1). The stations were deployed as three separate subarrays in two separate mobilizations. From June 2012 to April 2014, a 72-station seismic array was deployed across the Hangay dome in central Mongolia, 61 STS-2 sensors from Incorporated Research Institutions for Seismology–Program for the Array Seismic Studies of the Continental Lithosphere (IRIS-PASSCAL) and 7 STS-2.5 and 4 STS-2 sensors from the University of Florida (Fig. 1, detailed maps of the three subarrays are included in Ⓔ Fig. S1, available in the supplemental content to this article). Regional coverage was extended with two additional arrays deployed from August 2014 to June 2016, 26 stations (STS-2 sensors from IRIS-PASSCAL) to the north around the Lake Khövsgöl and Darkhad rifts and 14 stations (CMG-3T sensors from IRIS-PASSCAL) to the south at the intersection of the Mongolian and Gobi-Altai ranges (Fig. 1).

Station spacing was based on science objectives, accessibility, and security and is variable between and within the three subarrays. Minimum station spacing is 10–15 km, maximum 120–185 km, with an average station spacing of ~50 km across the 900 × 600 km aperture of the combined subarrays. The 72-station Hangay dome subarray is ~500 × 600 km. Station names in this subarray start with HD followed by station numbers (i.e., HDXX). The array contains two southwest–northeast transects across the Hangay with station spacing of 10–15 km embedded within a larger 2D array with station spacing between 25 and 80 km. Three of these stations, HD62, HD63, and HD64 sit above young volcanic cones at and near Tariat. The youngest volcanic cones are ~5000–7000 yr. B.P. (Chuvashova *et al.*, 2007; Hunt *et al.*, 2012) and contain mantle xenoliths. An additional eight stations, four to the north and four to the south, were deployed adjacent to the Bulnay and Gobi-Altai Bogd faults, respectively. The 26-station Khövsgöl subarray is 200 × 200 km. Station names in this subarray start with HV followed by station numbers (i.e., HVXX). The array is deployed across the Khövsgöl and Darkhad rifts in as much of a grid as feasible given access and very sparse population. Station spacing varies from 15 to 45 km with an average of 30 km. The 14-station Gobi-Altai subarray is ~250 by 150 km. Station names in this subarray start with AT followed by station numbers (i.e., ATXX). The array is deployed at the intersection of the Mongolian Altai and Gobi-Altai ranges marking a transition in the orientation of topography and strike-slip faults from ~N30°W in the Mongolian Altai to ~N80°W in the Gobi-Altai. Stations are deployed in a grid with station spacing varying ~40–60 km. Details for each station, location, recording dates, percent uptime, sensor orientation, data quality, and site characteristics are included in Ⓔ Table S1.

All stations were recorded by Q330 data loggers at 100 samples per second. Each station was powered by two 12 V 100 A hour-deep cycle batteries designed for solar systems and two 65 W solar panels. Sensor vaults were simple and easy to install. Sensors were placed on granite tiles, covered with an inverted plastic barrel, and buried ~0.5–1.0 m below the surface. Most sites are either directly on bedrock or within several meters to tens of meters from bedrock (see Ⓔ Table S1). Notable exceptions include HD09 in the Valley of the Lakes, a low-lying sedimentary basin south of the Hangay, and stations AT04, AT10, and AT15 deployed in dry lake sediments of the Gobi-Altai. HD72 was collocated with the Bulgan station of the Mongolian National Seismic Network, in a concrete vault ~2.5 m below the surface. Sensor orientations based on analysis of Rayleigh-wave polarization (Stachnik *et al.*, 2012) are within ±3.5° of north for the majority of stations (see Ⓔ Table S1 and Ⓔ Fig. S2). Exceptions due to installation error include HD35, which was misoriented by 18.6° ± 2.4° and AT14, HD20A, HD40, and HD45, which are off by ~9°–10°. Prescouting of the sites, the relative ease of installation, and the short distance between subsets of stations allowed teams to deploy two to three stations per day on average. All sites were accessible by four-wheel drive vehicle. Three teams deployed the 72 stations of the Hangay dome array over a two and a half week interval. Two teams deployed the 26 stations of the Khövsgöl array over an 11-day period. A single team deployed the Gobi-Altai array over a 10-day period. Abundant sun, relatively low precipitation, and good drainage resulted in 98% data recovery despite long cold winters (see Ⓔ Table S1).

Every temporary broadband deployment is unique with respect to field conditions and logistics. Mongolia is a large country (~1.6 million km^2) with relatively low population density (~2 people per km^2; Mendsaikhan *et al.*, 2012). Half of the 3 million people in Mongolia live in the capital Ulaanbaatar. A significant percentage of the population is nomadic, with extended family units moving two to four times a year depending on grazing conditions. The country has an extensive network of unimproved roads. The country is divided into 21 *aimags* (provinces). Aimag capitals are modest-size regional towns. Aimags are subdivided into *sums* (districts, sometimes transcribed soums) and *bags* (subdistricts or brigades, sometimes transcribed baghs) in terms of local governance. Each sum has a district seat, a regional town of variable size, generally bearing the name of the district. Bags generally (though not always) have a physical presence, a building, one or more gers, or set of storage buildings. Some bags

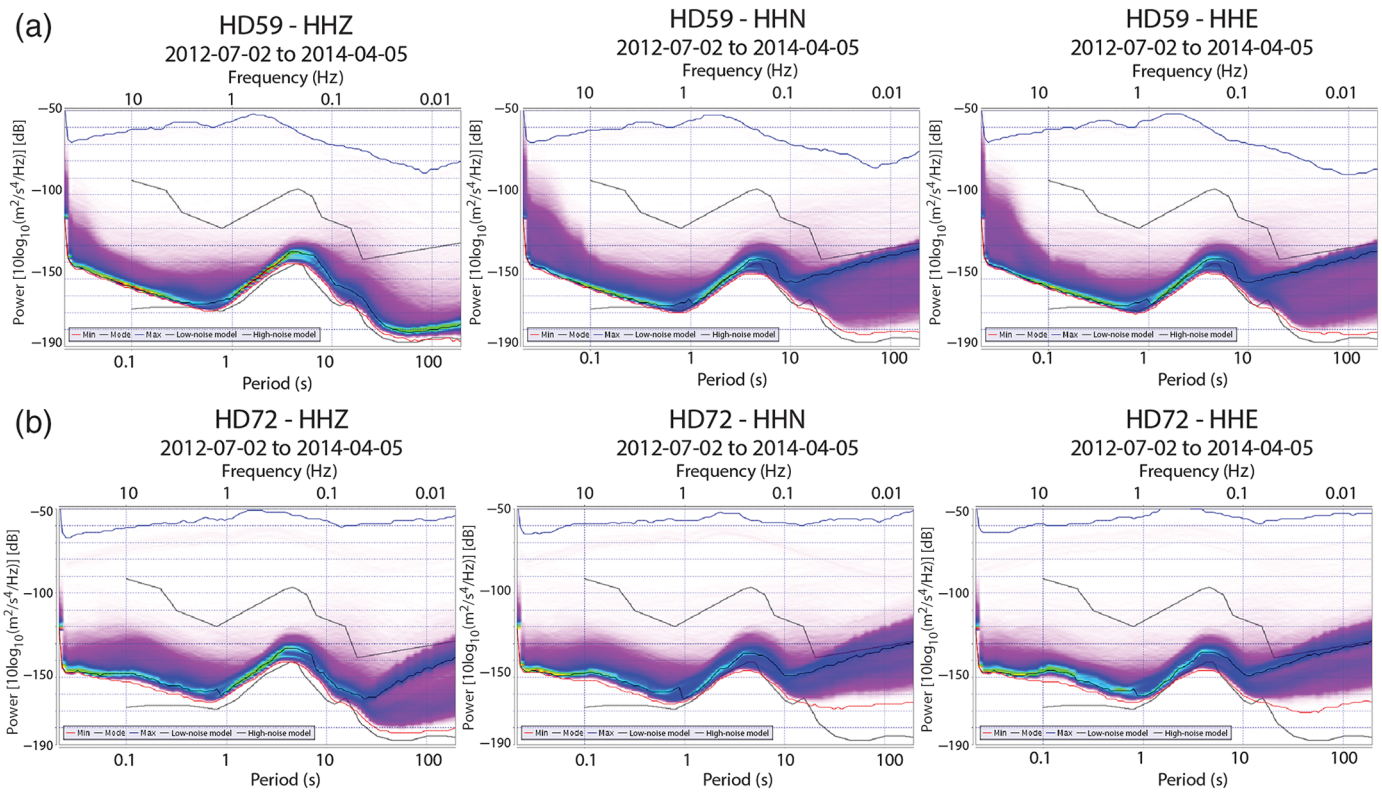

▲ **Figure 2.** Representative power spectral density (PSD) plots for stations in the central Mongolia seismic experiment. (a) PSD plots for station HD59 all three components, vertical (HHZ), north (HHN), east (HHE). Red line is the minimum, black line is the mode, and blue line is the maximum. Semiparallel gray lines are the high-noise (top line) and low-noise (bottom line) models (Peterson, 1993). Even with the shallow temporary vault, the vertical component is low noise at long periods. Not all stations were this quiet but many were. The horizontal components are noisier. (b) PSD plots for station HD72 all three components, vertical (HHZ), north (HHN), east (HHE). HD72 was deployed in a deep (2.5 m) concrete vault that also houses the Bulgan permanent station of the Mongolian National Seismic Network. The color version of this figure is available only in the electronic edition.

may have one or more families in residence year round, and many do not have any permanent residents. Approximately 15% of the country is protected in national parks, natural and historic monuments, natural reserves, or strictly protected areas with no established human influence requiring special permits. Permits to work in these areas are obtained from the appropriate government agency and take several weeks to process. For security, stations were primarily located in or near sums (district seats), bags with year-round residents, or with an extended family where some family members did not move or where summer and winter camps were located within a short distance. Several stations in the Gobi-Altai were installed in protected areas away from any human activity.

DATA QUALITY AND AVAILABILITY

Frequency-dependent noise levels for each station are evaluated using the power spectral density probability density function (PDF) noise toolkit provided by the IRIS Data Management Center (IRIS-DMC, 2014a). The noise characteristics of each station in three period bands: 0.1–1, 1–10, and 10–100 s, are included in Ⓔ Table S1. The majority of stations are either at the low-noise model (Peterson, 1993) or within 10 dB of the low-noise model in the microseism band between 1 and 10 s on all three components (Fig. 2). The noise characteristics of the stations in the shallow temporary vaults are similar to those of HD72 collocated with the permanent station Bulgan of the Mongolian National Seismic Network in a deep (2.5 m) concrete vault dug into bedrock (Fig. 2). The station vault is located in a remote area, 10.5 km away from the city of Bulgan, and ∼1 km from the Achuut River. Long-period noise at HD72 is most likely related to air circulation due to thermal variations in the permanent concrete vault.

At longer periods (10–100 s), the vertical channels are generally ∼20 dB above the low-noise model, and the horizontal components generally approach the high-noise model (Fig. 2). The predominant sources of noise at long periods are tilt related to atmospheric pressure changes and/or seasonal variations related to freeze-thaw cycles (Beauduin *et al.*, 1996; Wolin *et al.*, 2015). A number of stations exhibit a characteristic double band at long periods on the vertical channels (Fig. 3). Monthly spectrograms produced using the IRIS-DMC noise toolkit (IRIS-DMC, 2014b) show diurnal and seasonal variations in noise characteristics. Long-period noise is

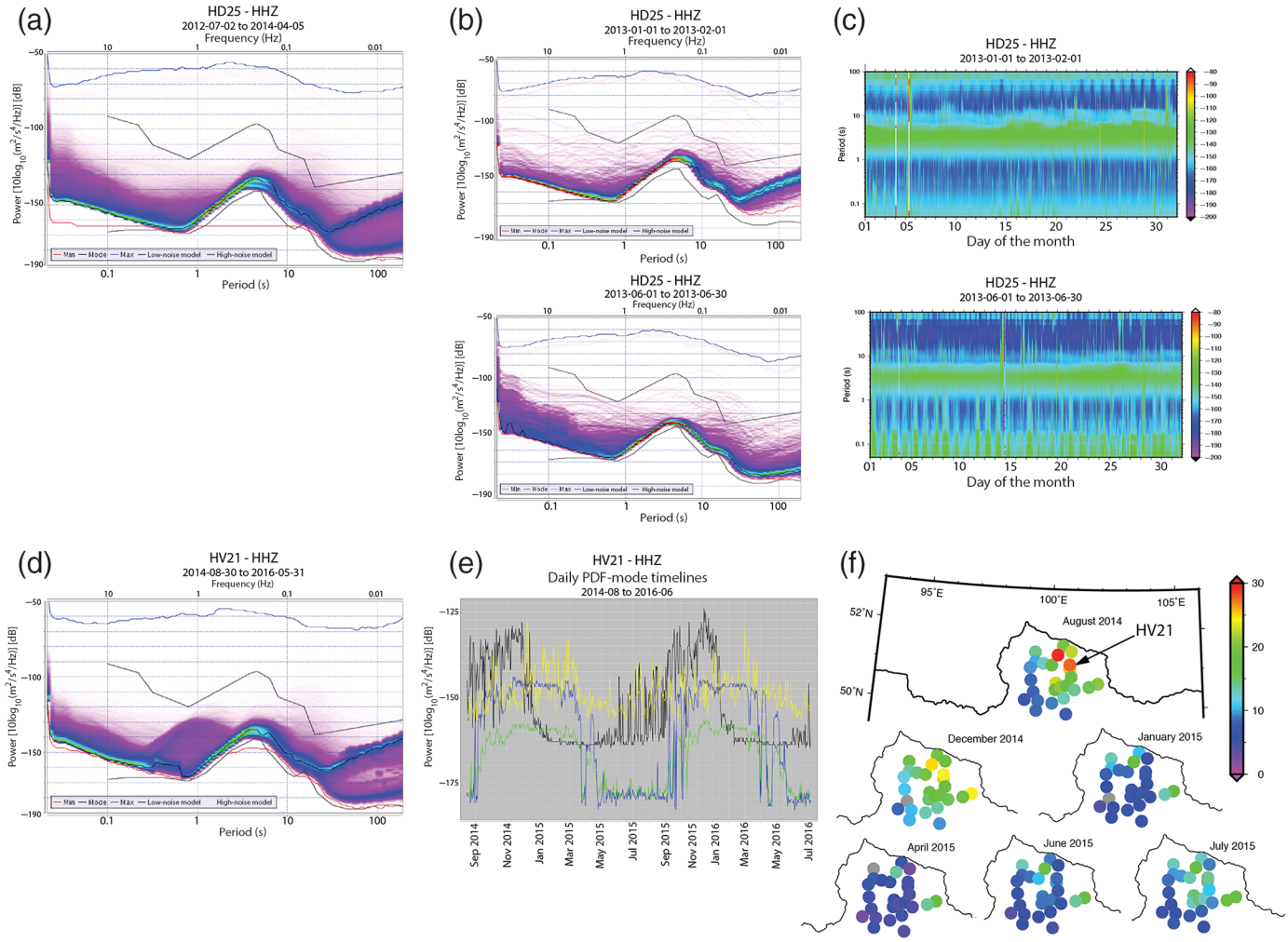

▲ **Figure 3.** (a) PSD plot for HD25 vertical component (HHZ) for 21-month deployment. PSD exhibits a double band at long periods associated with seasonal variations (winter and spring) characteristic of many of the stations in the central Mongolia seismic experiment. Red line is the minimum, black line is the mode, blue line is the maximum. Semi parallel gray lines are the high (top line) and low (bottom line) noise models (Peterson, 1993). (b) PSD plots for HD25 HHZ for January and June. Note difference in noise at long periods. (c) Spectrogram of the PSDs for HD25 in January and June shows higher long-period noise during the winter, and higher short-period noise and diurnal variations during the summer (color is in dB). (d) PSD for station HV21 (vertical component, HHZ) northeast shore of Lake Khövsgöl for 21-month deployment, PSD exhibits the characteristic double band at long periods and shoulder at short periods. (e) Daily mode timelines for HV21 (vertical component) from 100 to 1 s and (f) monthly mode (black, 1 s; yellow, 10 s; green, 30 s; blue, 100 s) of Khövsgöl subarray vertical component at 1 s (dB above the low-noise model) showing freeze thaw cycle (winter to spring) and reduced wave noise due to the frozen lake. The color version of this figure is available only in the electronic edition.

less in the summer and higher during the winter consistent with long-period noise due to winter freeze-thaw cycles.

At short periods (0.1–1 s), a significant number of stations are within 10 dB of the low-noise model (Fig. 2). The primary source of noise at short periods is either wind, or cultural noise associated with the movement of people, animals (goats, sheep, horses, cows, and yaks), and/or minor intermittent local car and truck traffic (Withers *et al.*, 1996; McNamara and Buland, 2004). Short-period noise is lower in the winter and higher and more variable during the summer (Fig. 3) consistent with increased levels of human and animal activity in the summer months. A subset of stations primarily located in the Khövsgöl subarray exhibits a shoulder between 1 and 3 s (Fig. 3). Daily PDF-mode timelines and monthly mode maps produced using the IRIS-DMC noise toolkit (IRIS-DMC, 2014b) show this is related to seasonal variations associated with prevailing wind direction and ice formation and melting in Lake Khövsgöl. 1 s noise drops dramatically between December and January as the lake freezes solidly and picks up again between June and July as lake melting occurs (Xu *et al.*, 2017; Anthony *et al.*, 2018).

All data from the central Mongolia seismic experiment are archived at the IRIS-DMC, network code XL-2012-2016 (Meltzer, 2012).

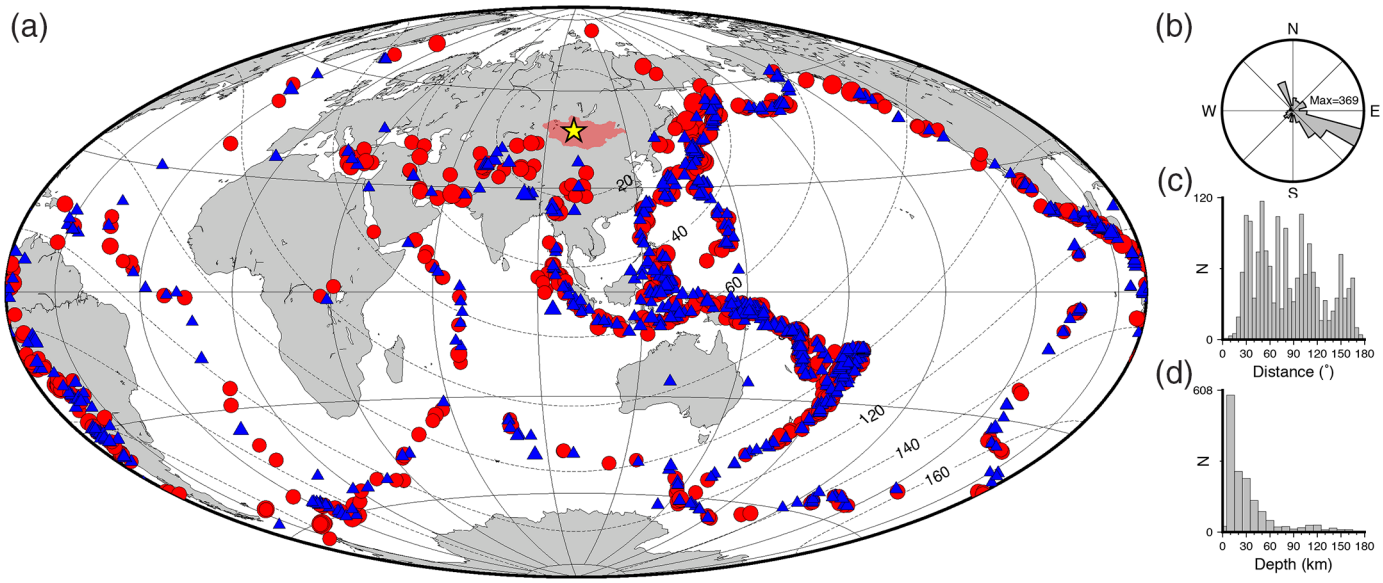

▲ **Figure 4.** (a) Global earthquakes $M_w \geq 5.5$ recorded by central Mongolia seismic experiment scaled by magnitude; 1745 earthquakes. Circles, July 2012–March 2014 earthquakes recorded by Hangay subarray; triangles, August 2014–June 2016 earthquakes recorded by the Khövsgöl and Gobi-Altai subarrays. (b) Rose diagram indicating azimuthal distribution, radius equal to 369 events (maximum). (c) Histogram of distance up to 180°. (d) Histogram of depth up to 180 km. In addition, the deep (~600 km) Sea of Okhotsk earthquake sequence in 2013 was recorded by the Hangay subarray. The color version of this figure is available only in the electronic edition.

INITIAL OBSERVATIONS: EVENTS OF INTEREST

The central Mongolia seismic experiment recorded 1745 events $M_w \geq 5.5$ (Fig. 4). Although events are dominated by earthquakes from the southwest Pacific along the Eurasian, Indo-Australian, and Pacific plate collisions, there is generally good azimuthal coverage over a range of distances. Like most temporary array deployments, the central Mongolia seismic experiment recorded a number of events of potential interest to a broad spectrum of the geoscience community. The array recorded the ground shaking associated with the airblast of the Chelyabinsk meteor on 15 February 2013. The Chelyabinsk meteor produced the largest airblast recorded by modern digital seismic networks with an estimated moment magnitude of M_w 3.60 (Heimann *et al.*, 2013) and surface-wave magnitude of M_s 3.7 ± 0.3 (Tauzin *et al.*, 2013). The Chelyabinsk airblast is superseded in size only by the Tunguska meteor in 1908 estimated at $M_w \sim 5.0$ (Ben-Menahem, 1975; Popova *et al.*, 2013). The Hangay dome subarray recorded the event at distances of 2500–3000 km along a back azimuth ~12° north of the meteor trajectory in the atmosphere (Berngardt *et al.*, 2015). Coupling between the ground and the shock wave produced as the meteor explodes generates Rayleigh waves that can be used to study the seismic source itself as well as Earth structure along the propagation path. The Hangay dome array also recorded the North Korean nuclear test on 12 February 2013. The Khövsgöl and Gobi-Altai arrays recorded the North Korean test on 6 January 2016. The two events have similar magnitudes 5.1 (U.S. Geological Survey [USGS], 2016a,b). The estimated yield of the events is 6–16.5 kt (Zhang and Wen, 2013).

Deep earthquakes are relatively rare and provide an opportunity to study the structure, rheology, state of stress, and rupture mechanisms associated with slabs that penetrate the mantle transition zone. The largest magnitude deep earthquake recorded to date is 24 May 2013 M_w 8.3 Sea of Okhotsk earthquake. This earthquake, at a depth of 609 km, was preceded by an M_w 7.7 event on 14 August at 583 km depth, and followed by two **M** 6.7 aftershocks, one on the same day as the mainshock and one several months later (30 September 2013), as well as a number of smaller aftershocks including eight aftershocks **M** 4.1–4.4 at 487–627 km depth within four days of the mainshock. A number of analyses using backprojection, directivity analysis, and waveform modeling have been carried out to study the rupture process, faulting mechanisms, slab heterogeneity, and the role of inherited zones of weakness from shallow intraplate faults on deep earthquake processes (Wei *et al.*, 2013; Ye *et al.*, 2013; Chen *et al.*, 2014; Meng *et al.*, 2014; Zhan *et al.*, 2014; Park and Ishii, 2015). The Hangay dome subarray sits at ~30° distance and a back azimuth of ~285° complementing teleseismic data from global stations and array data from Europe and North America used to examine the rupture processes associated with this sequence of events.

The array recorded 90 events in the 160°–180° distance range including the 1 April 2014 M_w 8.2 Iquique and 16 September 2015 M_w 8.3 Illapel earthquakes. The Iquique earthquake was preceded by an M_w 7.0 earthquake in March 2014 and five large aftershocks, $6.3 \leq M_w \leq 7.7$, occurred in the two days following the mainshock. The Illapel earthquake was followed by 13 large aftershocks (M_w between 6.1 and 7.0) within a 10-day period. These events are antipodal to central

Mongolia providing an opportunity to look at structure at the core–mantle boundary and can also be used to study rupture processes associated with these events.

The collision between India and Asia gives rise to the Himalaya and the Tibetan plateau and results in intercontinental seismogenesis over the ~2400 km Himalayan arc. The hazard from great earthquakes along the arc has the potential to impact millions of people across the Himalayan front in Pakistan, India, Nepal, Bhutan, and China/Tibet. The Himalayan megathrust ruptured in six great $\mathbf{M} \sim 8$ earthquakes between 1803 and 1950 (Chen and Molnar, 1977; Molnar and Pandey, 1989; Bilham *et al.*, 2001; Bilham, 2004). Elastic models of the strain energy available from plate convergence suggest this megathrust could rupture in an M_w 9.0 or larger earthquake (Feldl and Bilham, 2006). Historical ruptures pre-1800 have been identified but are challenging to study given the extent of surface rupture and the interplay of erosion and uplift in this setting (Lave, 2005; Ader *et al.*, 2012; Sapkota *et al.*, 2013; Bollinger *et al.*, 2014, 2016). The study of seismogenesis associated with megathrusts in continental collision zones lags behind studies in zones, as great earthquake ruptures were not captured by modern digital seismic and geodetic observations until the 25 April 2015 M_w 7.8 Gorkha earthquake.

The Gorkha earthquake ruptured a 120–165 km section of the Main Himalayan thrust (MHT) 82 km northwest of Kathmandu (USGS, 2016c). The 12 May 2015 M_w 7.3 aftershock ruptured an additional ~30 km section of the MHT at the eastern end of section that ruptured in the mainshock. An additional three large-magnitude aftershocks occurred, M_w 6.7 and 6.8 within a day of the mainshock, and an M_w 6.2 after the 12 May 2015 aftershock. Although there is broad agreement on the general rupture pattern, the detailed characteristics of the rupture, rupture process, initial rupture speed, acceleration and deceleration during rupture propagation, the location and number of subevents, and frequency-dependent energy release vary between studies (Avouac *et al.*, 2015; Fan and Shearer, 2015; Grandin *et al.*, 2015; Hayes *et al.*, 2015; Yagi and Okuwaki, 2015; Wang and Mori, 2016; Zhang *et al.*, 2016). The characteristics of the rupture are important as they influence ground shaking at high frequencies and in the case of Kathmandu basin resonance at low frequencies (Galetzka *et al.*, 2015). The details of the mainshock rupture and aftershock sequence can shed light on fault-slip behavior in continental collision zones and the extent to which their behavior is similar to or different from megathrusts in subduction zones. They also provide insight into depth-dependent fault strength, locking depth and the transition to down-dip stable sliding, the role of compositional and structural heterogeneity inherited during collision, as well as the role of fluids and/or thermal rheological control of fault behavior. Incorporating data from arrays at a range of azimuths and distances improves the resolution of backprojection results. The Khövsgöl and Gobi-Altai subarrays recorded the Gorkha earthquake and aftershocks at distances of 2000–3000 km (20°–24°) and back azimuth ~22°.

INITIAL RESULTS: LOCAL SEISMICITY HANGAY DOME

Mongolia is a major site of intracontinental earthquakes. Seismicity is most prominent along major strike-slip and thrust faults in the Mongolian Gobi-Altai Range, along the Bulnay fault, and in the northern rifts, but earthquakes are distributed over a large region of the country (Adiya *et al.*, 2003). Four great earthquakes with magnitude 8 and above occurred in a period of 53 yr (1905 M_w 8.0 Tsetserleg, 1905 M_w 8.3 Bulnay, 1931 M_w 8.0 Mongolian-Altai, and 1957 M_w 8.1 Gobi-Altai). Earthquakes with magnitudes between 5 and 8 have occurred with regularity and lower magnitude events are common (Baljinnyam *et al.*, 1993; Adiya *et al.*, 2003; Bayasgalan *et al.*, 2005). More than 50% of Mongolia's population lives in Ulaanbaatar. As the country's capital and only major city, the nation's major infrastructure, commercial and financial enterprises, universities, and government are all located in Ulaanbaatar, making the country and its citizens particularly vulnerable to seismic hazard posed by even a single nearby event. There are a large number of active faults in Mongolia capable of producing earthquakes above $M_w > 6.5$ (Bayasgalan *et al.*, 2005). In 1967, the **M** 7.4 Mogod earthquake ruptured only 250 km from Ulaanbaatar. Beginning in 2005, earthquake swarms were observed in the vicinity of Ulaanbaatar along the Hustai, Emeelt, Gunj, and Deren faults. Earthquake swarms in 2005 (472 events), 2009 (530 events), 2010 (781 events), 2012 (827 events), and 2013 (2184 events) account for a significant fraction of the seismicity in Mongolia in the last decade.

Our understanding of deformation and the earthquake cycle in intraplate settings remains far from complete. Although seismicity in Mongolia is generally thought to be related to deformation at the northern end of the India–Asia collision (Molnar and Tapponnier, 1975; Cunningham, 1998; Calais *et al.*, 2003), Mongolia sits 2000–3000 km north of the collisional zone. Both the Tibetan plateau, and Tarim and North China cratons lie between the collisional zone and Mongolia. The occurrence of numerous large to great earthquakes over decadal timescales does not match our understanding of the earthquake cycle. Analysis of the evolution of Coulomb stress failure after large earthquakes suggests that clusters of earthquakes can be triggered by previous events and that significant stress transfer takes place between continental faults hundreds of kilometers apart over timescales that span decades (Pollitz *et al.*, 2003). Geodynamic models incorporating basal tractions associated with mantle convection coupled to the lithosphere show that topography and lithospheric heterogeneity play a role in focusing strain in intracontinental regions (Ghosh *et al.*, 2013). With a long historical record of seismicity, new digital seismic and geodetic networks, and the arid climate and low erosion rates yielding remarkably well-preserved fault scarps and geomorphic expression of faulting, Mongolia is an excellent place to study intracontinental seismicity (Walker *et al.*, 2007, 2008, 2015; Rizza *et al.*, 2011, 2015; Arzhannikova *et al.*, 2015; Choi *et al.*, 2018).

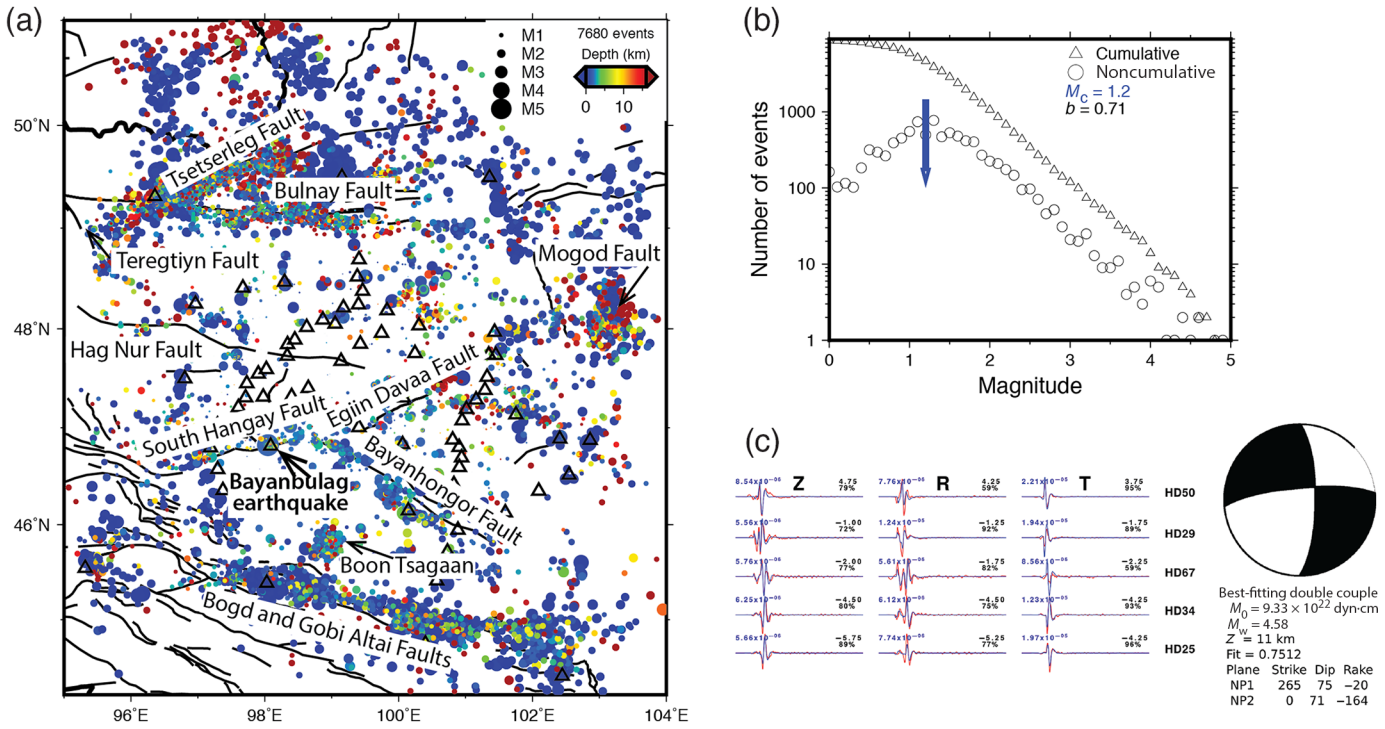

▲ **Figure 5.** (a) Local earthquakes recorded by the Hangay subarray during the 21-month deployment scaled by magnitude. (b) Magnitude versus frequency used to calculate magnitude of completeness (M_c = 1.2) and b-value (b = 0.71). (c) Regional moment tensor solution for the October 2012 M_w 4.58 Bayanbulag earthquake along the South Hangay fault. Fault plane strike of 265° is consistent with fault scarp visible at the surface. Three-component waveforms are shown for five closest stations to epicenter. Red lines, observed traces; blue lines, synthetic traces for best solution. The color version of this figure is available only in the electronic edition.

Here, we report preliminary earthquake locations for events recorded by the Hangay dome subarray determined through automatic processing using tools from the BRTT Antelope software (see Data and Resources). Automatic detections were picked using short-term average (STA) versus long-term average (LTA) ratios on vertical and horizontal components for P and S waves, respectively (P waves: 1–10 Hz, STA/LTA > 4.0; S waves: 1–5 Hz, STA/LTA > 4.0). Detections are associated with potential earthquake arrivals using a precomputed travel-time grid built using the ak135 velocity model. Hypocenter locations are determined via an iterative least-squares inversion of travel-time residuals (Pavlis *et al.*, 2004). Traditional Richter (local) magnitude (M_L) is calculated automatically for events recorded by a minimum of five stations with signal-to-noise ratio > 3. Events resulting from automatic detections with a minimum of 10 defining phases and magnitude greater than zero were reviewed by analysts and relocated in a simple local 1D velocity model (Fig. 5). Arrival times from 7680 events at local and regional distances indicate an average crustal velocity of V_P = 6.4 km/s and V_S = 3.6 km/s. The crossover distance to Pn and Sn reflects a thicker than average continental crust of ~50 km (Mordvinova *et al.*, 2007; Stachnik *et al.*, 2014; J. C. Stachnik *et al.*, unpublished manuscript, 2019; see Data and Resources). Seismicity is restricted to the upper 20 km of the crust with the majority of events locating in the upper 10 km. Magnitude of completeness (M_c) was estimated by the maximum curvature method (Wiemer and Katsumata, 1999; Wiemer and Wyss, 2000) to be 1.2, after a correction factor of 0.2 is applied as this method has been shown to underestimate M_c (Wiemer and Katsumata, 1999; Woessner and Wiemer, 2005). Using this M_c and the maximum-likelihood method for calculating b-values (Aki, 1965) and magnitude-binning width of 0.1, we calculate a b-value of 0.71. This b-value is less than the common value of 1.0 for tectonically active regions; it is more similar to b-values reported for intraplate settings (Okal and Sweet, 2007). Our estimation of M_c looks appropriate upon visual inspection (Fig. 5), but this b-value calculation could also reflect an incomplete earthquake catalog, inaccurate estimation of M_c, or variable tectonic stress states throughout the region. Further investigation of the final seismic catalog may indicate a variable spatial distribution of b-values.

The resulting earthquake locations clearly outline the Bulnay fault extending ~400 km laterally along the northern edge of the Hangay (Fig. 5). They also outline the adjacent Teregtiyn and Tsetserleg faults, both of which ruptured in 1905. Earthquakes recorded by the Hangay subarray outline the Bogd and other faults in the Gobi-Altai and a cluster of seismicity located close to Boon Tsagaan north of the Bogd fault in the Valley of the Lakes. Seismicity is also associated with the location of the 1967 Mogod earthquake northeast of the Hangay. In 1967, the **M** 7.4 Mogod earthquake ruptured

a 36 north–south right-lateral strike-slip fault (Tapponnier and Molnar, 1979; Khil'ko *et al.*, 1985; Huang and Chen, 1986; Baljinnyam *et al.*, 1993). An **M** 6.7 earthquake followed 15 days later on a southeast-striking reverse-fault located near the south end of the mainshock. In 1958, an **M** 6.2 earthquake occurred along strike ~50 km to the north and the region appears to be a source of persistent moderate-to-large events (Baljinnyam *et al.*, 1993; Bayasgalan *et al.*, 1999; Adiya *et al.*, 2003; Rogozhin *et al.*, 2008).

Although the Hangay has been described as aseismic, a number of small faults with various orientations and Quaternary offsets have been mapped within the Hangay (Cunningham, 2001; Walker *et al.*, 2008, 2015). The close station spacing of the Hangay dome subarray reveals seismicity within the Hangay, most notably on the South Hangay–Bayanhongor fault system and also along structures potentially associated with the Hag Nuur and Egiin Davaa faults as well as other faults within the Hangay (Fig. 5).

The South Hangay fault ruptured in the Bayanbulag earthquake on 3 October 2012. This event was well recorded by the Hangay dome subarray. The moment tensor solution yields M_w 4.58 and a source location of latitude 46.8232°, longitude 98.0662°, at 11.0 km depth (Fig. 5). The regional moment tensor solution was determined using Computer Programs in Seismology (Herrmann, 2013) using the local 1D velocity model, and three-component signals filtered in the 20–50 s band. The weighted variance reduction of more than 70% yields a stable solution with strike-slip motion along a fault striking 265° with a dip of 75° consistent with the observed fault trace at the surface. The mainshock was followed by more than 500 aftershocks outlining the steeply southeast-dipping fault plane. The epicentral region is sparsely populated. Ground shaking was felt locally and foundations and walls cracked in the town of Bayanbulag, but overall damage was minimal.

The surface trace of the South Hangay fault is visible in Google Earth images and exhibits clear geomorphic expression in satellite imagery and in the field (Walker *et al.*, 2007). The left-lateral strike-slip fault extends over 350 km. To the east, a clear band of seismicity links the South Hangay fault to the Bayanhongor fault (Fig. 5). To the west, a band of seismicity links the South Hangay fault to east–west-trending left-lateral faults associated with transpressive structures that emerge from within the Valley of the Lakes associated with deformation for which Gobi-Atlai joins the Mongolia Altai. Several northwest–southeast bands of seismicity are observed north of the western trace of the South Hangay fault. These bands of seismicity align roughly along strike of the trace of the Teregtiyn fault farther north.

Within the interior of the Hangay, there is sufficient seismicity to suggest that parts of the Hangay are deforming, rather than behaving as a rigid block (Fig. 5). Seismicity is observed in the vicinity of the Egiin Davaa fault, a north–south-trending normal fault, exhibiting an 80 km continuous 4–4.5 m fault scarp. The Egiin Davaa fault is estimated to have ruptured in an **M** 7.3–7.7 earthquake ~4000 yr ago (Walker *et al.*, 2015). There is a southwest–northeast band of seismicity on the north-central flank of the Hangay trending toward the eastern end of the Bulnay fault and a band of seismicity in the eastern Hangay trending northwest–southeast along strike of the projection of the Hag Nuur fault.

Preliminary locations of seismicity recorded by the Hangay dome subarray suggest that active faults within the Hangay accommodate strain within the larger India–Asia collision and should be incorporated in hazard analysis for Mongolia. The extent to which these distributed bands of seismicity collapse to more discrete faults will be better determined in a subsequent joint inversion for 3D velocity and earthquake location.

SUMMARY

The central Mongolia seismic experiment was designed to characterize the structure of the lithosphere and sublithospheric mantle to understand the origin of high topography in the continental interior of central Asia. Analyses of *Ps* and *Sp* receiver functions and shear-wave splitting measurements from the combined arrays, joint inversion of Rayleigh-wave dispersion and forward-scattered *P* waves, and coda-wave attenuation beneath the Hangay have been completed (Stachnik *et al.*, 2014; Meltzer *et al.*, 2015; Cui *et al.*, 2016; Russo *et al.*, 2016; Ganbat *et al.*, 2017; J. C. Stachnik *et al.*, unpublished manuscript, 2019; see Data and Resources), and results are in preparation for publication. Finite-frequency teleseismic body-wave tomography and joint inversion of local earthquakes for location and 3D velocity are in progress. Initial results from local seismicity suggest that active faults within the Hangay accommodate strain within the larger India–Asia collision. Data captured during the recording window of the central Mongolia seismic experiment can be used to study deep Earth structure using antipodal events from South America, and rupture processes associated with large-magnitude subduction earthquakes offshore Chile, the Gorkha, Nepal, earthquake sequence, and the deep Sea of Okhotsk earthquakes. Data recorded by the array have the potential to contribute to studies of surface and atmospheric processes, and nuclear monitoring.

DATA AND RESOURCES

The data described in this article were collected as part of the central Mongolia seismic experiment using Incorporated Research Institutions for Seismology–Program for the Array Seismic Studies of the Continental Lithosphere (IRIS-PASSCAL) instruments and instruments from the University of Florida. Data can be obtained from the IRIS Data Management Center available at http://www.iris.edu/dms/nodes/dmc/ (network code XL-2012-2016; doi: http://dx.doi.org/10.7914/SN/XL_2012). Faults in Figure 5 are from Tomurtogoo (1999), Geological Map of Mongolia, Mongolian Academy of Sciences, scale: 1:1,000,000, Ulaanbaatar. Site characteristics in Ⓔ Table S1 (available in the supplemental content

to this article) are from local field observations and Tomurtogoo (1999), Geological Map of Mongolia, Mongolian Academy of Sciences, scale: 1:1,000,000, Ulaanbaatar. Maps and figures were made using the Generic Mapping Tools v.5.2.1 available at http://gmt.soest.hawaii.edu (Wessel *et al.*, 2013). The other information about BRTT Antelope software can be found at http://www.brtt.com (last accessed June 2018). The unpublished manuscript by J. C. Stachnik, A. Meltzer, S. Souza, U. Munkhuu, B. Tsaagan, and R. M. Russo (2019), "Airy-compensated high topography within a continental interior: Hangay dome, Mongolia," submitted to *Geophys. Res. Lett.*

ACKNOWLEDGMENTS

The authors gratefully acknowledge the assistance and support of families and local government officials in Huvsgul, Zavkhan, Bayankhongor, Uvurkhangai, Arkhangai, and Bulgan Aimags. Without their help, this work would not have been possible. The authors also acknowledge the excellent support of the administrative and technical support staff of the Institute for Astronomy and Geophysics of the Mongolian Academy of Sciences. The bulk of the instruments used in the field program was provided by the Program for the Array Seismic Studies of the Continental Lithosphere (PASSCAL) facility of the Incorporated Research Institutions for Seismology (IRIS) through the PASSCAL Instrument Center at New Mexico Tech with support from the National Science Foundation under Cooperative Agreement EAR-1261681 and by the Department of Energy National Nuclear Security Administration. This work was supported by the National Science Foundation Earth Sciences Continental Dynamics Program Award Numbers EAR-1009680 and EAR-1111515. The authors thank the anonymous reviewers for helpful comments to improve the article.

REFERENCES

Adachi, S., and F. Kimura (2007). A 36-year climatology of surface cyclogenesis in East Asia using high-resolution reanalysis data, *Sola* **3,** 113–116, doi: 10.2151/sola.2007-029.

Ader, T., J. P. Avouac, J. Liu-Zeng, H. Lyon-Caen, L. Bollinger, J. Galetzka, J. Genrich, M. Thomas, K. Chanrad, S. N. Sapkota, *et al.* (2012). Convergence rate across the Nepal Himalaya and interseismic coupling on the Main Himalayan thrust: Implications for seismic hazard, *J. Geophys. Res.* **117,** no. 4, 1–16, doi: 10.1029/2011JB009071.

Adiya, M., D. Ankhtsetseg, Ts. Baasanbat, G. Bayar, Ch. Bayarsaikhan, D. Erdenezul, D. Mungunsuren, A. Munkhsaikhan, D. Munkhuu, R. Narantsetseg, *et al.* (2003). *One Century of Seismicity in Mongolia (1900–2000)*, T. Dugarmaa and A. Schlupp (Editors), Research Centre of Astronomy & Geophysics of the Mongolian Academy of Sciences (RCAG), Mongolia and Laboratoire de Teledetection et Risque Sismique, BP12, Bruyères-le-Châtel, France.

Aki, K. (1965). Maximum likelihood estimate of b in the formula $\log N = a - bM$ and its confidence limits, *Bull. Earthq. Res. Inst.* **43,** 237–239.

Ancuta, L. D., R. W. Carlson, D. A. Ionov, and P. K. Zeitler (2014). Geochemistry and geochronology of the lower crust beneath central Mongolia, *American Geophysical Union, Fall Meeting 2014*, San Francisco, California, 15–19 December, Abstract Number T21A–4557.

Ancuta, L. D., P. K. Zeitler, B. D. Idleman, and B. T. Jordan (2018). Whole-rock $^{40}Ar/^{39}Ar$ geochronology, geochemistry, and stratigraphy of intraplate Cenozoic volcanic rocks, central Mongolia, *GSA Bull.* **130,** nos. 7/8, 1397–1408, doi: 10.1130/B31788.1.

Anthony, R. E., A. T. Ringler, and D. C. Wilson (2018). The widespread influence of Great Lakes microseisms across the midwestern United States revealed by the 2014 polar vortex, *Geophys. Res. Lett.* **45,** 3436–3444.

Arzhannikova, A. V., R. Vassallo, S. G. Arzhannikov, and M. Jolivet (2015). Morphotectonics and paleoseismology of the eastern end of the Bolnay fault (Mongolia), *Russ. Geol. Geophys.* **56,** 1484–1490.

Avouac, J.-P., L. Meng, S. Wei, T. Wang, and J.-P. Ampuero (2015). Lower edge of locked Main Himalayan thrust unzipped by the 2015 Gorkha earthquake, *Nature Geosci.* **8,** no. 9, 708–711, doi: 10.1038/ngeo2518.

Badarch, G., W. Dickson Cunningham, and B. F. Windley (2002). A new terrane subdivision for Mongolia: Implications for the Phanerozoic crustal growth of Central Asia, *J. Asian Earth Sci.* **21,** no. 1, 87–110, doi: 10.1016/S1367-9120(02)00017-2.

Baljinnyam, I., A. Bayasgalan, B. A. Borisov, A. Cisternas, M. G. Dem'yanovich, L. Ganbataar, V. M. Kochetkov, R. A. Kurushin, P. Molnar, H. Philip, *et al.* (1993). Ruptures of major earthquakes and active deformation in Mongolia and its surroundings, *Geol. Soc. Am. Memoir* **181,** doi: 10.1130/MEM181.

Barry, T. L., A. D. Saunders, P. D. Kempton, B. F. Windley, M. S. Pringle, D. Dorjnamjaa, and S. Saandar (2003). Petrogenesis of Cenozoic basalts from Mongolia: Evidence for the role of asthenospheric versus metasomatized lithospheric mantle sources, *J. Petrol.* **44,** no. 1, 55–91, doi: 10.1093/petrology/44.1.55.

Bayasgalan, A., J. Jackson, and D. McKenzie (2005). Lithosphere rheology and active tectonics in Mongolia: Relations between earthquake source parameters, gravity and GPS measurements, *Geophys. J. Int.* **163,** no. 3, 1151–1179, doi: 10.1111/j.1365-246X.2005.02764.x.

Bayasgalan, A., J. James, J.-F. Ritz, and S. Carretier (1999). Field examples of strike-slip fault terminations in Mongolia and tectonic significance, *Tectonics* **18,** no. 3, 394–411.

Beauduin, R., P. Lognonné, J. P. Montagner, S. Cacho, J. F. Karczewski, and M. Morand (1996). The effects of the atmospheric pressure changes on seismic signals or how to improve the quality of a station, *Bull. Seismol. Soc. Am.* **86,** no. 6, 1760–1769.

Ben-Menahem, A. (1975). Source parameters of the Siberian explosion of June 30, 1908, from analysis and synthesis of seismic signals at four stations, *Phys. Earth Planet. In.* **11,** no. 1, 1–35, doi: 10.1016/0031-9201(75)90072-2.

Berngardt, O. I., N. P. Perevalova, A. A. Dobrynina, K. A. Kutelev, N. V. Shestakov, V. F. Bakhtiarov, O. A. Kusonsky, R. V. Zagretdinov, and G. A. Zherebtsov (2015). Toward the azimuthal characteristics of ionospheric and seismic effects of "Chelyabinsk" meteorite fall according to the data from coherent radar, GPS, and seismic networks, *J. Geophys. Res.* **120,** no. 12, 10,754–10,771, doi: 10.1002/2015JA021549.

Bilham, R. (2004). Earthquakes in India and the Himalaya: Tectonics, geodesy and history, *Ann. Geophys.* **47,** nos. 2/3, 839–858, doi: 10.4401/ag-3338.

Bilham, R., V. K. Gaur, and P. Molnar (2001). Himalayan seismic hazard, *Science* **293,** 1442–1444, doi: 10.1126/science.1062584.

Bollinger, L., S. N. Sapkota, P. Tapponnier, Y. Klinger, M. Rizza, J. Van Der Woerd, D. R. Tiwari, R. Pandey, A. Bitri, and S. Bes de Berc (2014). Estimating the return times of great Himalayan earthquakes in eastern Nepal: Evidence from the Patu and Bardibas strands of the Main Frontal thrust, *J. Geophys. Res.* **119,** no. 9, 7123–7163, doi: 10.1002/2014JB010970.

Bollinger, L., P. Tapponnier, S. N. Sapkota, and Y. Klinger (2016). Slip deficit in central Nepal: Omen for a pending repeat of the 1344 AD earthquake? *Earth Planets Space* **68,** 1–12, doi: 10.1186/s40623-016-0389-1.

Burtin, A., L. Bollinger, J. Vergne, R. Cattin, and J. L. Nábělek (2008). Spectral analysis of seismic noise induced by rivers: A new tool to monitor spatiotemporal changes in stream hydrodynamics, *J. Geophys. Res.* **113,** no. 5, 1–14, doi: 10.1029/2007JB005034.

Butler, R., and S. Tsuboi (2010). Antipodal seismic observations of temporal and global variation at Earth's inner-outer core boundary, *Geophys. Res. Lett.* **37,** no. 11, 1–5, doi: 10.1029/2010GL042908.

Butler, R., T. M. Brocher, and J. A. Rial (1986). Inner core experiments: Teleseismic exploration of the antipode, *Eos Trans. AGU* **67,** no. 8, 89–94, doi: 10.1029/EO067i008p00089-01.

Calais, E., M. Vergnolle, V. San'kov, A. Lukhnev, A. Miroshnitchenko, S. Amarjargal, and J. Déverchère (2003). GPS measurements of crustal deformation in the Baikal-Mongolia area (1994–2002): Implications for current kinematics of Asia, *J. Geophys. Res.* **108,** no. B10, 2501, doi: 10.1029/2002JB002373.

Carlson, R. W., and D. A. Ionov (2014). Lithospheric mantle contribution to high topography in central Mongolia, *American Geophysical Union, Fall Meeting 2014*, San Francisco, California, 15–19 December, Abstract Number T21A–4556.

Caves, J. K., M. J. Winnick, S. A. Graham, D. J. Sjostrom, A. Mulch, and C. P. Chamberlain (2015). Role of the westerlies in Central Asia climate over the Cenozoic, *Earth Planet. Sci. Lett.* **428,** 33–43, doi: 10.1016/j.epsl.2015.07.023.

Chen, W.-P., and P. Molnar (1977). Seismic moments of major earthquakes and the average rate of slip in central Asia, *J. Geophys. Res.* **82,** no. 20, 2945–2969.

Chen, Y., L. Wen, and C. Ji (2014). A cascading failure during the 24 May 2013 great Okhotsk deep earthquake, *J. Geophys. Res.* **119,** 3035–3049, doi: 10.1002/2013JB010926.

Choi, J.-H., Y. Klinger, M. Ferry, J.-F. Ritz, R. Kurtz, M. Rizza, L. Bollinger, B. Davaasambuu, N. Tsend-Ayush, and S. Demberel (2018). Geologic inheritance and earthquake rupture processes: The 1905 M ≥ 8 Tsetserleg-Bulnay strike-slip earthquake sequence, Mongolia, *J. Geophys. Res.* **123,** 1925–1953, doi: 10.1002/2017JB013962.

Chung, Y.-S., K. D. Hage, and E. R. Reinelt (1976). On Lee cyclogenesis and airflow in the Canadian Rocky Mountains and the East Asian Mountains, *Mon. Weather Rev.* **104,** no. 7, 879–891, doi: 10.1175/1520-0493(1976)104<0879:OLCAAI>2.0.CO;2.

Chuvashova, I., S. Rasskazov, T. Yasnygina, E. Saranina, and N. Fefelov (2007). Holocene volcanism in central Mongolia and northeast China: Asynchronous decompressional and fluid melting of the mantle, *J. Volcanol. Seismol.* **1,** no. 6, 372–396, doi: 10.1134/S0742046307060024.

Cui, Z., A. Meltzer, J. Stachnik, K. M. Fischer, R. M. Russo, U. Munkhuu, and T. Baasanbat (2016). Structure of the upper mantle and mantle transition zone in central Mongolia, *2016 Fall Meeting, AGU*, San Francisco, California, 12–16 December, T11B–2625.

Cunningham, W. D. (1998). Lithospheric controls on late Cenozoic construction of the Mongolian Altai, *Tectonics* **17,** no. 6, 891–902, doi: 10.1029/1998TC900001.

Cunningham, W. D. (2001). Cenozoic normal faulting and regional doming in the southern Hangay region, central Mongolia: Implications for the origin of the Baikal rift province, *Tectonophysics* **331,** no. 4, 389–411, doi: 10.1016/S0040-1951(00)00228-6.

Fan, W., and P. M. Shearer (2015). Detailed rupture imaging of the 25 April 2015 Nepal earthquake using teleseismic *P* waves, *Geophys. Res. Lett.* **42,** no. 14, 5744–5752, doi: 10.1002/2015GL064587.

Feldl, N., and R. Bilham (2006). Great Himalayan earthquakes and the Tibetan plateau, *Nature* **444,** no. 7116, 165–170, doi: 10.1038/nature05199.

Galetzka, J., D. Melgar, J. F. Genrich, J. Geng, S. Owen, E. O. Lindsey, X. Xu, Y. Bock, J.-P. Avouac, L. B. Adhikari, *et al.* (2015). Slip pulse and resonance of the Kathmandu basin during the 2015 Gorkha earthquake, Nepal, *Science* **349,** no. 6252, 1091–1095, doi: 10.1126/science.aac6383.

Ganbat, B., A. Meltzer, J. C. Stachnik, and U. Munkhuu (2017). Estimation of coda wave attenuation in the Hangay Dome, central Mongolia, *International Conf. on Astronomy and Geophysics Mongolia*, Ulaanbaatar, Mongolia, 20–22 July 2017.

Ghosh, A., W. E. Holt, and L. Wen (2013). Predicting the lithospheric stress field and plate motions by joint modeling of lithosphere and mantle dynamics, *J. Geophys. Res.* **118,** no. 1, 346–368, doi: 10.1029/2012JB009516.

Grandin, R., M. Vallée, C. Satriano, R. Lacassin, Y. Klinger, M. Simoes, and L. Bollinger (2015). Rupture process of the M_w = 7.9 2015 Gorkha earthquake (Nepal): Insights into Himalayan megathrust segmentation, *Geophys. Res. Lett.* **42,** no. 20, 8373–8382, doi: 10.1002/2015GL066044.

Hayes, G. P., R. W. Briggs, W. D. Barnhart, W. L. Yeck, D. E. McNamara, D. J. Wald, J. L. Nealy, H. M. Benz, R. D. Gold, K. S. Jaiswal, *et al.* (2015). Rapid characterization of the 2015 M_w 7.8 Gorkha, Nepal, earthquake sequence and its seismotectonic context, *Seismol. Res. Lett.* **86,** no. 6, 1557–1567, doi: 10.1785/0220150145.

Heimann, S., A. Gonzalez, R. Wang, S. Cesca, and T. Dahm (2013). Seismic characterization of the Chelyabinsk meteor's terminal explosion, *Seismol. Res. Lett.* **84,** no. 6, 1021–1025, doi: 10.1785/0220130042.

Herrmann, R. B. (2013). Computer programs in seismology: An evolving tool for instruction and research, *Seismol. Res. Lett.* **84,** no. 6, 1081–1088, doi: 10.1785/0220110096.

Hsu, L., N. J. Finnegan, and E. E. Brodsky (2011). A seismic signature of river bedload transport during storm events, *Geophys. Res. Lett.* **38,** no. 13, doi: 10.1029/2011GL047759.

Huang, J., and W.-P. Chen (1986). Source mechanisms of the Mogod earthquake sequence of 1967 and the event of 1974 July 4 in Mongolia, *Geophys. J. Roy. Astron. Soc.* **84,** 361–379.

Hunt, A. C., I. J. Parkinson, N. B. W. Harris, T. L. Barry, N. W. Rogers, and M. Yondon (2012). Cenozoic volcanism on the Hangai Dome, central Mongolia: Geochemical evidence for changing melt sources and implications for mechanisms of melting, *J. Petrol.* **53,** no. 9, 1913–1942, doi: 10.1093/petrology/egs038.

Incorporated Research Institutions for Seismology–Data Management Center (IRIS-DMC) (2014a). *Data Services Products: Noise Toolkit PDF-PSD Noise Toolkit PDF/PSD bundle*, doi: 10.17611/DP/NTK.2.

Incorporated Research Institutions for Seismology–Data Management Center (IRIS-DMC) (2014b). *Data Services Products: The IRIS DMC Noise Toolkit*, doi: 10.17611/DP/NTK.1.

Ionov, D. A. (2007). Compositional variations and heterogeneity in fertile lithospheric mantle: Peridotite xenoliths in basalts from Tariat, Mongolia, *Contrib. Mineral. Petrol.* **154,** no. 4, 455–477, doi: 10.1007/s00410-007-0203-y.

Jahn, B.-M. (2004). The central Asian orogenic belt and growth of the continental crust in the Phanerozoic, *Geol. Soc. Lond. Spec. Publ.* **226,** no. 1, 73–100, doi: 10.1144/gsl.sp.2004.226.01.05.

Khil'ko, S. D., R. A. Kurushin, V. M. Kochetkov, I. Balzhinnyam, and D. Monkoo (1985). Strong earthquakes, paleoseismogeological and macroseismic data, in *Earthquakes and the Bases for Seismic Zoning of Mongolia*, Transactions 41, The Joint Soviet-Mongolian Scientific Geological Research Expedition, Nauka, Moscow, Russia, 19–83.

Lave, J. (2005). Evidence for a Great Medieval earthquake (1100 A.D.) in the central Himalayas, Nepal, *Science* **307,** no. 5713, 1302–1305, doi: 10.1126/science.1104804.

McNamara, D. E., and R. P. Buland (2004). Ambient noise levels in the continental United States, *Bull. Seismol. Soc. Am.* **94,** no. 4, 1517–1527.

Meltzer, A. (2012). *Central Mongolia Seismic Experiment, Mongolia*, International Federation of Digital Seismograph Networks, Other/Seismic Network, doi: 10.7914/SN/XL_2012.

Meltzer, A., L. D. Ancuta, R. W. Carlson, J. K. Caves, C. P. Chamberlain, J. C. Gosse, B. D. Idleman, D. A. Ionov, K. T. McDannell, M. Tamra, *et al.* (2015). Betwixt and between: Structure and evolution of central Mongolia, *American Geophysical Union, Fall Meeting 2015*, San Francisco, California, 14–18 December, Abstract Number T22A–05.

Mendsaikhan, S., G. Gerelt-Od, B. Erdenesuren, B. Ganbat, and K. Bajiikhuu (2012). *Mongolian Statistical Yearbook 2011*, National Statistical Office of Mongolia, 462 pp.

Meng, L., J. P. Ampuero, and R. Burgmann (2014). The 2013 Okhotsk deep-focus earthquake: Rupture beyond the metastable olivine wedge and thermally controlled rise time near the edge of a slab, *Geophys. Res. Lett.* **41,** 3779–3785, doi: 10.1002/2014GL059968.

Molnar, P., and M. R. Pandey (1989). Rupture zones of great earthquakes in the Himalayan region, *Proc. Indian Acad. Sci. Earth Planet. Sci.* **98,** no. 1, 61–70, doi: 10.1007/BF02880376.

Molnar, P., and P. Tapponnier (1975). Cenozonic tectonics of Asia effects of a continental collision, *Science* **189,** no. 4201, 419–426.

Mordvinova, V. V., A. Deschamps, T. Dugarmaa, J. Deverchére, M. Ulziibat, V. A. Sankov, A. A. Artem'ev, and J. Perrot (2007). Velocity structure of the lithosphere on the 2003 Mongolian-Baikal transect from *SV* waves, *Izvestiya Phys. Solid Earth* **43,** no. 2, 119–129, doi: 10.1134/S1069351307020036.

Okal, E. A., and J. R. Sweet (2007). Frequency-size distributions for intraplate earthquakes, in *Continental Intraplate Earthquakes: Science, Hazard, and Policy Issues*, S. Stein and S. Mazzotti (Editors), Geol. Soc. Am. Spec. Pap. 425, 59–71, doi: 10.1130/2007.2425(05).

Park, S., and M. Ishii (2015). Inversion for rupture properties based upon 3-D directivity effect and application to deep earthquakes in the Sea of Okhotsk region, *Geophys. J. Int.* **203,** no. 2, 1011–1025, doi: 10.1093/gji/ggv352.

Pavlis, G. L., F. Vernon, D. Harvey, and D. Quinlan (2004). The generalized earthquake-location (GENLOC) package: An earthquake-location library, *Comput. Geosci.* **30,** nos. 9/10, 1079–1091, doi: 10.1016/j.cageo.2004.06.010.

Penny, S., G. H. Roe, and D. S. Battisti (2010). The source of the mid-winter suppression in storminess over the North Pacific, *J. Climate* **23,** no. 3, 634–648, doi: 10.1175/2009JCLI2904.1.

Peterson, J. (1993). Observations and modeling of seismic back-ground noise, *U.S. Geol. Surv. Open-File Rept. 93-322*, 95 pp.

Petit, C., J. Déverchère, and D. Fairhead (2002). Deep structure and mechanical behavior of the lithosphere in the Hangai-Hövsgöl region, Mongolia: New constraints from gravity modeling, *Earth Planet. Sci. Lett.* **197,** 133–149.

Petit, C., C. Tiberi, A. Deschamps, and J. Déverchère (2008). Teleseismic traveltimes, topography and the lithospheric structure across central Mongolia, *Geophys. Res. Lett.* **35,** no. 11, 1–5, doi: 10.1029/2008GL033993.

Pollitz, F., M. Vergnolle, and E. Calais (2003). Fault interaction and stress triggering of twentieth century earthquakes in Mongolia, *J. Geophys. Res.* **108,** no. B10, 2503, doi: 10.1029/2002JB002375.

Popova, O. P., P. Jenniskens, V. Emel, A. Kartashova, E. Biryukov, S. Khaibrakhmanov, V. Shuvalov, Y. Rybnov, A. Dudorov, V. I. Grokhovsky, *et al.* (2013). Chelyabinsk airburst, damage assessment, meteorite recovery, and characterization, *Science* **342,** 1069–1073, doi: 10.1126/science.1242642.

Poupinet, G., A. Souriau, and L. Jenatton (1993). A test on the Earth's core–mantle boundary structure with antipodal data: Example of Fiji-Tonga earthquakes recorded in Tamanrasset, Algeria, *Geophys. J. Int.* **113,** no. 3, 684–692, doi: 10.1111/j.1365-246X.1993.tb04660.x.

Retailleau, L., N. M. Shapiro, J. Guilbert, M. Campillo, and P. Roux (2014). Antipodal focusing of seismic waves observed with the USArray, *Geophys. J. Int.* **199,** no. 2, 1030–1042, doi: 10.1093/gji/ggu309.

Rial, J. A., and V. F. Cormier (1980). Seismic waves at the epicenter's antipode, *J. Geophys. Res.* **85,** no. 80, 2661–2668.

Rizza, M., J. F. Ritz, R. Braucher, R. Vassallo, C. Prentice, S. Mahan, S. McGill, A. Chauvet, S. Marco, M. Todbileg, *et al.* (2011). Slip rate and slip magnitudes of past earthquakes along the Bogd left-lateral strike-slip fault (Mongolia), *Geophys. J. Int.* **186,** no. 3, 897–927, doi: 10.1111/j.1365-246X.2011.05075.x.

Rizza, M., J. F. Ritz, C. Prentice, R. Vassallo, R. Braucher, C. Larroque, A. Arzhannikova, S. Arzhannikov, S. Mahan, M. Massault, *et al.* (2015). Earthquake geology of the Bulnay fault (Mongolia), *Bull. Seismol. Soc. Am.* **105,** no. 1, 72–93, doi: 10.1785/0120140119.

Roe, G. (2009). On the interpretation of Chinese loess as a paleoclimate indicator, *Quaternary Res.* **71,** no. 2, 150–161, doi: 10.1016/j.yqres.2008.09.004.

Rogozhin, E. A., V. S. Imaev, O. P. Smekalin, and D. P. Schwartz (2008). Tectonic position and geological manifestations of the Mogod (central Mongolia), January 5, 1967, earthquake (a view after 40 years), *Izvestiya Phys. Solid Earth* **44,** no. 8, 666–677, doi: 10.1134/S1069351308080065.

Roth, D. L., N. J. Finnegan, E. E. Brodsky, K. L. Cook, C. P. Stark, and H. W. Wang (2014). Migration of a coarse fluvial sediment pulse detected by hysteresis in bedload generated seismic waves, *Earth Planet. Sci. Lett.* **404,** 144–153, doi: 10.1016/j.epsl.2014.07.019.

Russo, R. M., A. Meltzer, J. C. Stachnik, U. Munkhuu, B. Tsaagan, and Z. Cui (2016). Upper mantle fabrics of the Mongolian central Asian orogenic belt: Observations and inferences from shear wave splitting intensity measurements, *2016 Fall Meeting, AGU*, San Francisco, California, 12–16 December, T33B–3028.

Sapkota, S. N., L. Bollinger, Y. Klinger, P. Tapponnier, Y. Gaudemer, and D. Tiwari (2013). Primary surface ruptures of the great Himalayan earthquakes in 1934 and 1255, *Nature Geosci.* **6,** 71–76, doi: 10.1038/ngeo1669.

Schlupp, A., and A. Cisternas (2007). Source history of the 1905 great Mongolian earthquakes (Tsetserleg, Bolnay), *Geophys. J. Int.* **169,** no. 3, 1115–1131, doi: 10.1111/j.1365-246X.2007.03323.x.

Schmandt, B., R. C. Aster, D. Scherler, V. C. Tsai, and K. Karlstrom (2013). Multiple fluvial processes detected by riverside seismic and infrasound monitoring of a controlled flood in the Grand Canyon, *Geophys. Res. Lett.* **40,** no. 18, 4858–4863, doi: 10.1002/grl.50953.

Şengör, A. M. C., B. A. Natal'in, and V. S. Burtman (1993). Evolution of the Altaid tectonic collage and Palaeozoic crustal growth in Eurasia, *Nature* **364,** no. 6453, 299–307, doi: 10.1038/364299a0.

Stachnik, J. C., A. Meltzer, S. Souza, U. Munkhuu, B. Tsaagan, and R. M. Russo (2014). Lithospheric structure beneath the Hangay dome, central Mongolia, *American Geophysical Union, Fall Meeting 2014*, San Francisco, California, 15–19 December, Abstract Number T21A–4555.

Stachnik, J. C., A. F. Sheehan, D. W. Zietlow, Z. Yang, J. Collins, and A. Ferris (2012). Determination of New Zealand ocean bottom seismometer orientation via Rayleigh-wave polarization, *Seismol. Res. Lett.* **83,** no. 4, 704–713, doi: 10.1785/0220110128.

Stosch, H. G., D. A. Ionov, I. S. Puchtel, S. J. Galer, and A. Sharpouri (1995). Lower crystal xenoliths from Mongolia and their bearing on the nature of the deep dust beneath central Asia, *Lithos* **36,** nos. 3/4, 227–242.

Tapponnier, P., and P. Molnar (1979). Active faulting and Cenozoic tectonics of the Tien Shan, Mongolia, and Baykal regions, *J. Geophys. Res.* **84,** no. B7, 3425–3459.

Tauzin, B., E. Debayle, C. Quantin, and N. Coltice (2013). Seismoacoustic coupling induced by the breakup of the 15 February 2013 Chelyabinsk meteor, *Geophys. Res. Lett.* **40,** no. 14, 3522–3526, doi: 10.1002/grl.50683.

Tomurtogoo, O. (Editor) (1999). *Geological Map of Mongolia*, Mongolian Academy of Sciences, scale 1:1,000,000.

U.S. Geological Survey (USGS) (2016a). M 5.1 nuclear explosion—24km ENE of Sungjibaegam, North Korea, available at http://earthquake.usgs.gov/earthquakes/eventpage/usc000f5t0#general_region (last accessed March 2016).

U.S. Geological Survey (USGS) (2016b). M 5.1 nuclear explosion—21km ENE of Sungjibaegam, North Korea, available at http://earthquake.usgs.gov/earthquakes/eventpage/us10004bnm#general_region (last accessed March 2016).

U.S. Geological Survey (USGS) (2016c). M 7.8–36km E of Khudi, Nepal, available at http://earthquake.usgs.gov/earthquakes/eventpage/us20002926#general_region (last accessed March 2016).

Walker, R. T., E. Molor, M. Fox, and A. Bayasgalan (2008). Active tectonics of an apparently aseismic region: Distributed active strike-slip faulting in the Hangay Mountains of central Mongolia, *Geophys. J. Int.* **174,** no. 3, 1121–1137, doi: 10.1111/j.1365-246X.2008.03874.x.

Walker, R. T., E. Nissen, E. Molor, and A. Bayasgalan (2007). Reinterpretation of the active faulting in central Mongolia, *Geology* **35,** no. 8, 759–762, doi: 10.1130/G23716A.1.

Walker, R. T., K. W. Wegmann, A. Bayasgalan, R. J. Carson, J. Elliott, M. Fox, E. Nissen, R. A. Sloan, J. M. Williams, and E. Wright (2015). The Egiin Davaa prehistoric rupture, central Mongolia: A large magnitude normal faulting earthquake on a reactivated fault with little cumulative slip located in a slowly deforming intraplate setting, in *Seismicity, Fault Rupture and Earthquake Hazards in Slowly Deforming Regions*, Geol. Soc. Lond. Spec. Publ. 432, 187–212, doi: 10.1144/SP432.4.

Wang, D., and J. Mori (2016). Short-period energy of the 25 April 2015 M_w 7. 8 Nepal earthquake determined from backprojection using four arrays in Europe, China, Japan, and Australia, *Bull. Seismol. Soc. Am.* **106,** no. 1, 1–8, doi: 10.1785/0120150236.

Wei, S., D. Helmberger, Z. Zhan, and R. Graves (2013). Rupture complexity of the M_w 8.3 Sea of Okhotsk earthquake: Rapid triggering of complementary earthquakes? *Geophys. Res. Lett.* **40,** no. 19, 5034–5039, doi: 10.1002/grl.50977.

Wessel, P., W. H. F. Smith, R. Scharroo, J. Luis, and F. Wobbe (2013). Generic Mapping Tools: Improved version released, *Eos Trans. AGU* **94,** no. 45, 409–410, doi: 10.1002/2013EO450001.

Wiemer, S., and K. Katsumata (1999). Spatial variability of seismicity parameters in aftershocks zones, *J. Geophys. Res.* **104,** no. B6, 13,135–13,151.

Wiemer, S., and M. Wyss (2000). Minimum magnitude of completeness in earthquake catalogs: Examples from Alaska, the western United States, and Japan, *Bull. Seismol. Soc. Am.* **90,** no. 4, 859–869, doi: 10.1785/0119990114.

Wilhem, C., B. F. Windley, and G. M. Stampfli (2012). The Altaids of central Asia: A tectonic and evolutionary innovative review, *Earth Sci. Rev.* **113,** nos. 3/4, 303–341, doi: 10.1016/j.earscirev.2012.04.001.

Windley, B. F., and M. B. Allen (1993). Mongolian plateau: Evidence for a late Cenozoic mantle plume under central Asia, *Geology* **21,** 295–298.

Windley, B. F., D. V. Alexeiev, W. Xiao, A. Kröner, and G. Badarch (2007). Tectonic models for accretion of the central Asian orogenic belt, *J. Geol. Soc.* **164,** 31–47, doi: 10.1144/0016-76492006-022.

Withers, M. M., R. C. Aster, C. J. Young, and E. P. Chael (1996). High-frequency analysis of seismic background noise as a function of wind speed and shallow depth, *Bull. Seismol. Soc. Am.* **86,** no. 5, 1507–1515.

Woessner, J., and S. Wiemer (2005). Assessing the quality of earthquake catalogues: Estimating the magnitude of completeness and its uncertainty, *Bull. Seismol. Soc. Am.* **95,** no. 2, 684–698, doi: 10.1785/0120040007.

Wolin, E., S. van der Lee, T. A. Bollmann, D. A. Wiens, J. Revenaugh, F. A. Darbyshire, A. W. Frederiksen, S. Stein, and M. E. Wysession (2015). Seasonal and diurnal variations in long-period noise at SPREE stations: The influence of soil characteristics on shallow stations' performance, *Bull. Seismol. Soc. Am.* **105,** no. 5, 2433–2452.

Xu, Y., K. D. Koper, and R. Burlacu (2017). Lakes as a source of short-period (0.5–2 s) microseisms, *J. Geophys. Res.* **122,** 8241–8256, doi: 10.1002/2017JB014808.

Yagi, Y., and R. Okuwaki (2015). Integrated seismic source model of the 2015 Gorkha, Nepal, earthquake, *Geophys. Res. Lett.* **42,** no. 15, 6229–6235, doi: 10.1002/2015GL064995.

Yanovskaya, T. B., and V. M. Kozhevnikov (2003). 3D *S*-wave velocity pattern in the upper mantle beneath the continent of Asia from Rayleigh wave data, *Phys. Earth Planet. In.* **138,** nos. 3/4, 263–278, doi: 10.1016/S0031-9201(03)00154-7.

Yarmolyuk, V. V., E. A. Kudryashova, A. M. Kozlovsky, and V. A. Lebedev (2008). Late Cenozoic volcanism of Khangai (central Mongolia): Evidence for recent orogeny in central Asia, *Dokl. Earth Sci.* **422,** no. 1, 1032–1036, doi: 10.1134/S1028334X08070064.

Ye, L., T. Lay, H. Kanamori, and K. D. Koper (2013). Energy release of the 2013 M_w 8.3 Sea of Okhotsk earthquake and deep slab stress heterogeneity, *Science* **341,** 1380–1384, doi: 10.1126/science.1242032.

Zhan, Z., D. V. Helmberger, H. Kanamori, and P. M. Shearer (2014). Supershear rupture in a M_w 6.7 aftershock of the 2013 Sea of Okhotsk earthquake, *Science* **345,** no. 6193, 204–207, doi: 10.1126/science.1252717.

Zhang, H., S. Van Der Lee, and Z. Ge (2016). Multiarray rupture imaging of the devastating 2015 Gorkha, Nepal, earthquake sequence, *Geophys. Res. Lett.* **43,** no. 2, 584–591, doi: 10.1002/2015GL066657.

Zhang, M., and L. Wen (2013). High-precision location and yield of North Koreas 2013 nuclear test, *Geophys. Res. Lett.* **40,** no. 12, 2941–2946, doi: 10.1002/grl.50607.

Zorin, Y. A., E. K. Turutanov, V. M. Kozhevnikov, S. V. Rasskazov, and A. V. Ivanov (2006). Cenozoic upper mantle plumes in east Siberia and central Mongolia and subduction of the Pacific plate, *Dokl. Earth Sci.* **409,** no. 5, 723–726, doi: 10.1134/S1028334X06050096.

Anne Meltzer
Joshua C. Stachnik
Department of Earth and Environmental Sciences
Lehigh University
1 West Packer Avenue
Bethlehem, Pennsylvania 18015 U.S.A.
ameltzer@lehigh.edu
jcstachnik@gmail.com

Demberel Sodnomsambuu
Ulziibat Munkhuu
Baasanbat Tsagaan
Mungunsuren Dashdondog
Institute of Astronomy and Geophysics
Mongolian Academy of Sciences
POB-152
Ulaanbaatar 13343
Mongolia
demberel@iag.ac.mn
ulzibat@iag.ac.mn
baasanbat@iag.ac.mn
mongon@iag.ac.mn

Raymond Russo
Department of Geological Sciences
University of Florida
241 Williamson Hall
P.O. Box 112120
Gainesville, Florida 32611-2120 U.S.A.
rrusso@ufl.edu

Published Online 10 April 2019